HIGH-REDSHIFT RADIO GALAXIES FROM THE MOLONGLO CATALOGUE

P. J. McCarthy
The Observatories of the Carnegie Institution of Washington, 813 Santa Barbara Street, Pasadena, California 91101

V. K. Kapahi
Giant Meter-Wave Radio Telescope Project, T.I.F.R., Poona University Campus, Ganeshkhind, Pune 41107, India

W. van Breugel
Institute of Geophysics and Planetary Physics, Lawrence Livermore National Laboratory, Livermore, California 94550

C. R. Subrahmanya
Giant Meter-Wave Radio Telescope Project, T.I.F.R., Poona University Campus, Ganeshkhind, Pune 41107, India
Received 3 April 1990; revised 15 June 1990

ABSTRACT

We report the results of radio and optical observations of a sample of southern hemisphere radio galaxies selected from the Molonglo Reference Catalogue. The sources were selected to have 408 MHz flux densities greater than 0.9 Jy and low-frequency spectral indices steeper than -0.9. VLA 6 cm maps and optical identifications of 13 sources are presented. All of these sources are identified with faint galaxies, many of which have extended optical structures with morphologies characteristic of high-redshift ($z > 0.8$) radio galaxies. Long-slit spectroscopic observations have yielded redshifts for 11 of the galaxies, 5 of which are at $z > 2$. The most distant source in the present sample, 0316 − 257, has a redshift of 3.13, while the median redshift for the sample is 1.6. Our results for this subsample suggest that our total sample of 150 sources may contain $\sim$ 40 galaxies with $z > 2$. We have imaged four of our galaxies having $z > 2$ in the light of Lyα. Three of these have highly extended Lyα emission distributed along their radio axes.

I. INTRODUCTION

The past three years have seen an explosion in our empirical knowledge of radio galaxies at high redshift. This has arisen both from a rapid increase in the number of galaxies known at large redshifts (and in the limiting redshift) as well as from detailed cross-spectral studies of well-defined samples. The 3CR sample of extragalactic radio sources (Bennet 1962), defined by a limiting flux density of $S_{178} = 9$ Jy contains 25 radio galaxies with $z > 1$, 15 with $z > 1.5$ and a single galaxy with $z > 2$ (Spinrad, private communication). The B2/1 Jy sample of Allington-Smith (1982) has a larger fraction of galaxies with $z > 1$ but is highly restricted in its sky coverage. As a result only nine galaxies with $z > 1$ and two with $z > 2$ have been identified (Allington-Smith *et al.* 1988; Lilly 1989). Some of the most spectacular results have come from the 4C "ultrasteep" sample of Chambers *et al.* (1988, 1989). These sources have 178 MHz flux densities greater than 2.0 Jy and are selected to have α_{178}^{5000} steeper than -1.0. Chamber's sample of $\sim$40 objects has yielded $\sim$eight galaxies with $z > 2$, making it the largest sample of galaxies at such high redshifts. Spectroscopic observations of 175 objects in the much weaker (mJy level at 1.4 GHz) LBDS sample (Windhorst *et al.* 1984) have yielded two galaxies with $1 < z < 2$ and a single galaxy with $z > 2$ (Windhorst 1990). High-frequency selected samples (e.g., Parkes Selected Regions, Dunlop *et al.* 1989; MIT/GB, Lawrence *et al.* 1986) are still highly incomplete, although Spinrad and Dickinson (private communication) have had substantial success with the MG survey and McCarthy *et al.* (unpublished) have detected two Parkes Selected Region galaxies with $z > 1.5$. McCarthy and Djorgovski (unpublished) have also had success in identifying $z > 2$ radio galaxies from the B3 sample.

The success of the "1 Jy" class samples and the "ultrasteep" selection criterion motivated us to define a sample of sources combining these two criteria. Our sample is originally drawn from the 408 MHz Molonglo Reference Catalogue (Large *et al.* 1981). A complete subset of roughly 700 sources in a restricted declination range ($-30° < \delta < -20°$) and having $S_{408} > 0.95$ Jy was observed by one of us (Subrahmanya, in preparation) using the Molonglo Synthesis Telescope at 843 MHz. Snapshot observations at several hour angles resulted in accurate positions which were used to search for optical identifications on film copies of the SRC-J sky survey plates. From these we have further selected a subset of 150 sources that have no optical identifications (or plate limit objects) and have steep radio spectra, with $\alpha_{408}^{843} < -0.9$. Such a sample may be expected to combine the best characteristics of the 1 Jy and ultrasteep samples with respect to finding galaxies at large redshifts.

The choice of flux densities comes from consideration of the differential source counts. At $S_{408} \sim 1$ Jy the counts exceed non-evolving models by the largest factor (e.g., Condon 1984), and hence these must be the most rapidly evolving population of sources, as pointed out by Allington-Smith (1982) and others. The 1 Jy sources should then contain the most luminous objects at essentially all redshifts.

The spectral index criterion is more subtle. There have long been claims of a correlation between spectral index and luminosity (Laing and Peacock 1980, and references therein) in strong source samples such as the 3CR. Because of the tight correlation between redshift and luminosity in such samples it is not clear whether the primary correlation is between redshift and spectral index or luminosity and spectral index. Peacock (1985), however, has noted that in strong source surveys at high radio frequencies (e.g., the 2.7

 0004-6256/90/041014-14$00.90

GHz all sky survey) that contain a much higher fraction of compact steep spectrum sources, the observed $P-\alpha$ correlation is quite weak. A further complication is introduced by the curvature of the radio spectra. A large fraction of the extended sources have spectra that steepen with increasing frequency. Thus high-redshift (and hence high-luminosity) sources will appear steeper at a fixed observed frame frequency even if there is no intrinsic correlation between P and α. Gopal-Krishna (1988) has shown that when comparing strong sources in the 408 MHz all sky survey (Robertson 1973) and the 1 Jy sources in the Allington-Smith (1982) sample at higher redshifts, the differences in their spectral indices is largely the result of spectral curvature. This suggests that the apparent increase of α with z is partly an artifact of spectral curvature. van Breugel and McCarthy (1990) have reexamined the P–α correlation in the complete 3CR sample after transforming all of the spectral indices to 1.4 GHz in the rest frame. They find only a weak residual trend of α with P. Furthermore, Kapahi and Kulkarni (1990) have recently pointed out that the residual trend could arise from a selection effect related to the steepening slope of the radio luminosity function with increasing luminosity. This results in the preferential selection of ultrasteep spectrum sources of high luminosity in a low-frequency catalog.

Chambers and Miley (1990), however, argue that the rapid drop in the fraction of sources identified on the POSS plates as a function of α (Tielens *et al.* 1979) supports a correlation between P and α. Since nearly all of the 3CR sources with $z > 0.5$ are unidentified on the POSS, this result does not require that a large fraction of the steep sources lies at redshifts much larger than one. Furthermore, since the identification statistics are based on observed-frame spectral indices, the correlation could result from spectral curvature and the above-mentioned selection effect. Observations of larger samples are clearly required to determine the reality and importance of any correlation between P and α. Regardless of the question of the P–α relation, the empirical $\alpha_{\rm observed}$–z correlation can be used to select high-redshift sources in analogy to an optical color selection criteria.

II. OBSERVATIONS

a) Radio Imaging

All of the radio sources were observed with the VLA at 6 cm with the array in its hybrid A/B configuration which is well suited to southern sources. Each source was observed for roughly five minutes at a single hour angle with frequent observations of calibrator sources interleaved. CLEANed and self-calibrated maps were made for each source using standard processing techniques. Details of the radio observations and results will be presented by Kapahi *et al.* at a later date.

The 6 cm maps of all of the sources that were observed spectroscopically are presented in Figs. 1(a)–1(m). The resolution varies between roughly 1".3 and 2" and the typical rms noise in each map is 0.15 mJy. The sources parameters are given in Table I. The derived radio positions are given in Table II. For sources without detected central components, we list the midpoint between the two hotspots rather than the flux-density weighted centroid.

We have supplemented the flux densities from the Molonglo Reference Catalogue (Large *et al.* 1981) and the Molonglo Synthesis Telescope observations by Subrahmanya at 843 MHz with measurements from other radio catalogs. All of the sources presented here were detected in the University of Texas Radio Astronomy Observatory survey at 365 MHz (Douglas *et al.* 1980). Some of these sources were detected at higher frequencies at Parkes but their flux densities are so uncertain that we have not used them in our determination of spectral indices. At high frequencies we use our own 4.86 GHz flux densities integrated over the entire source (Table I, column 2). These values may under-represent structure on scales larger than $\sim 30''$ and hence the flux densities should be regarded as lower limits. Nearly all of the sources in our complete sample are small enough so that this is not a large source of error. This was confirmed by examining the visibilities, which showed no evidence for a dramatic increase in flux density at short spacings. For most sources the spectral data is insufficient to allow a reliable determination of the spectral index at a fixed rest-frame frequency. Only α_{408}^{4860}, determined between fixed observed-frame frequencies, is listed in Table I. In the strictest sense, however, the listed values should be treated as lower limits (i.e., the spectra could be flatter) for the reason given above. The spectral indices determined between these two frequencies are, in general, significantly steeper than those derived from the 408–843 MHz data alone, as would be expected from spectral curvature at high frequencies.

b) Optical Imaging

Deep optical images were obtained for 20 sources in the R.A. range $20^{\rm h} < \alpha < 4^{\rm h}$ with the Las Campanas 2.5 m Du Pont telescope in July 1989. Each field was observed with a Gunn–Thuan r filter. Several short integrations (300–900 s) were made and combined to give total integration times of typically 2400 s. The observing conditions were photometric, but the seeing was mediocre (1.4–1.8 FWHM). The detector was a TI 800×800 CCD used in a 2×2 on-chip binning mode to give 0".337 pixels. The optical images were flattened using dark sky flats and were calibrated using standard techniques. Individual processed images of each field were shifted into registration and added. The radio sources were identified from astrometry of stars in each field whose positions were determined relative to a grid of SAO stars from the POSS. The typical rms errors of the primary astrometric solutions were 0".7 in each coordinate. The final rms errors for the derived galaxy positions are roughly 1". Of the 20 sources imaged, four were identified with quasars, three with relatively bright galaxies ($r\sim19$–20), two remained unidentified, and the remaining 11 were identified with galaxies fainter than $r = 21$. The magnitudes were determined through small apertures, typically 4" in diameter. Larger apertures were used for the more extended objects (e.g., 0156 − 252, 2104 − 242). The positions for each of the galaxy identifications (designated by O) are listed in Table II, along with the position of a bright secondary reference star. The reference stars are designated by an upper-case letter corresponding to those in the figures. Grey-scale reproductions of each field are presented in Figs. 2(a)–2(m). Each field shown in Fig. 2 is $85''\times85''$, except that of 0316 − 257 [Fig. 2(m)] which is $126''\times126''$. In each image the position of the identification is marked by two lines, the orientation of which reflects the position angle of the extended radio source. A secondary reference star is identified by a capital letter in each field.

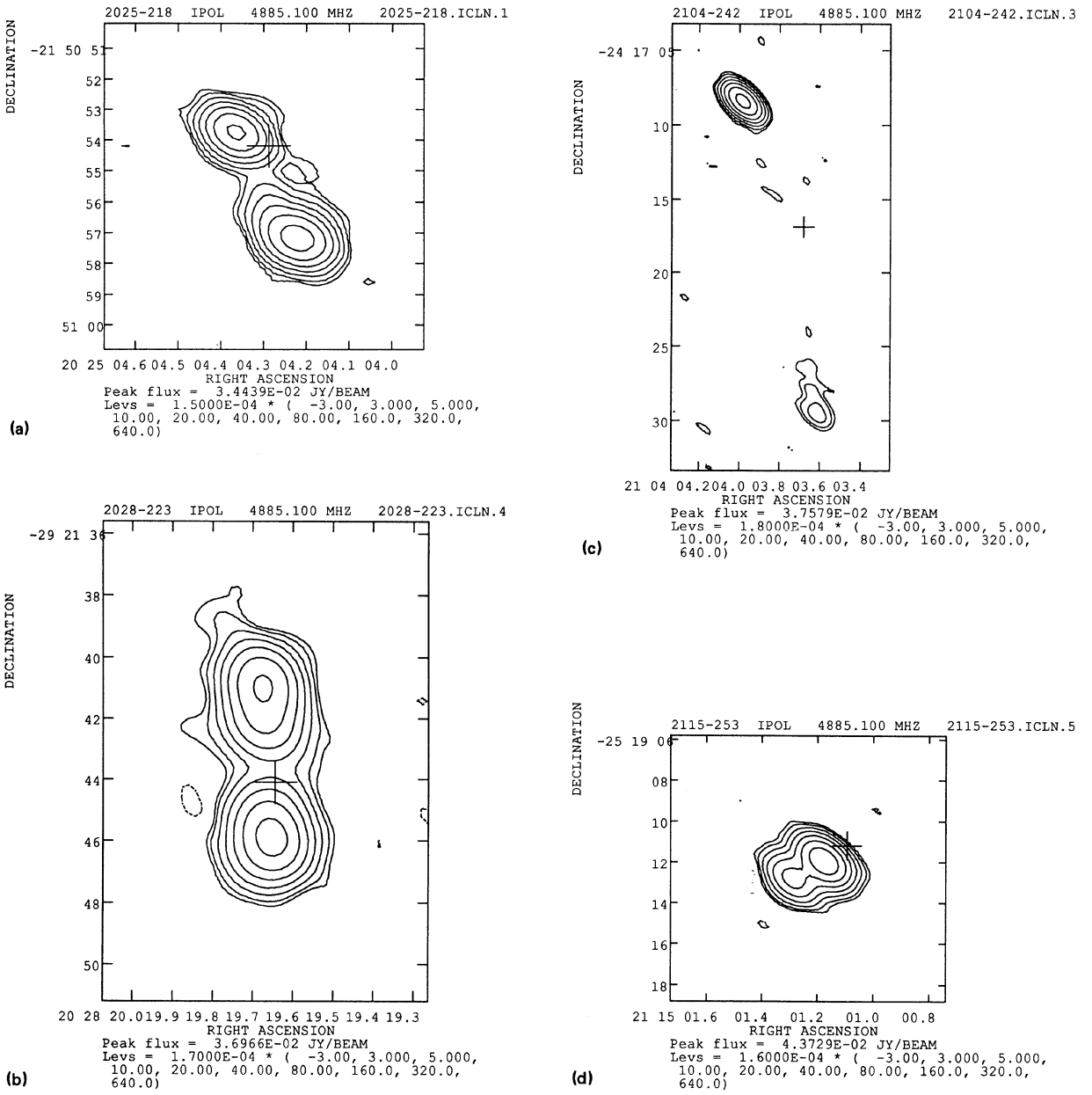

FIG. 1. (a)–(d) 6 cm VLA maps of 2025 – 218, 2028 – 293, 2104 – 242, and 2115 – 253. The average resolution of each map is 1".3 and the position of the optical identification is marked with a cross. The contour levels are – 3, 3, 5, 10, 20, 40, 80, 160, 320, and 640 times the rms noise per beam which is typically 0.16 mJy. (e)–(h) 6 cm VLA maps of 2200 – 252, 2226 – 224, 2247 – 248, and 2303 – 252. (i)–(l) 6 cm VLA maps of 0030 – 219, 0034 – 235, 0156 – 252, and 0203 – 209. (m) A 6 cm VLA map of 0316 – 257.

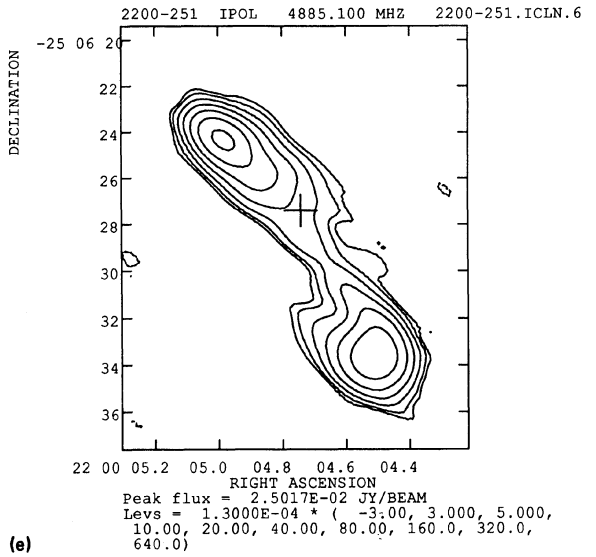

(e)

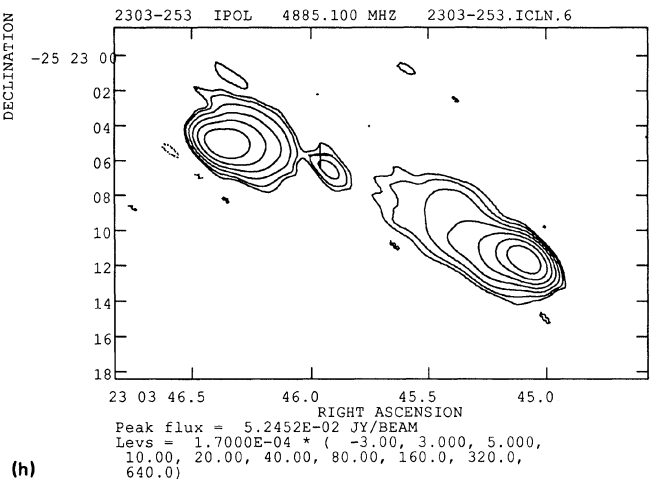

(h)

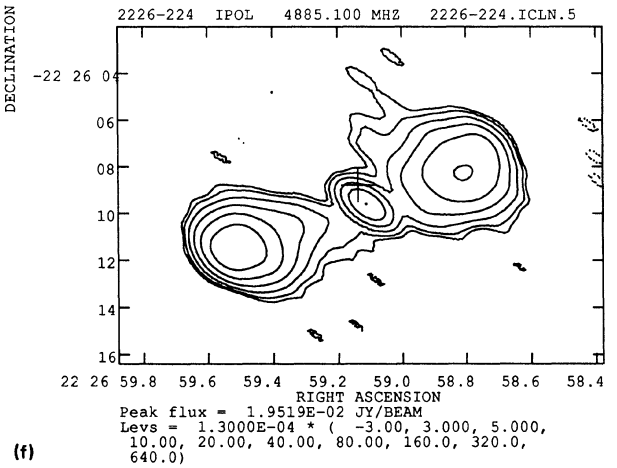

(f)

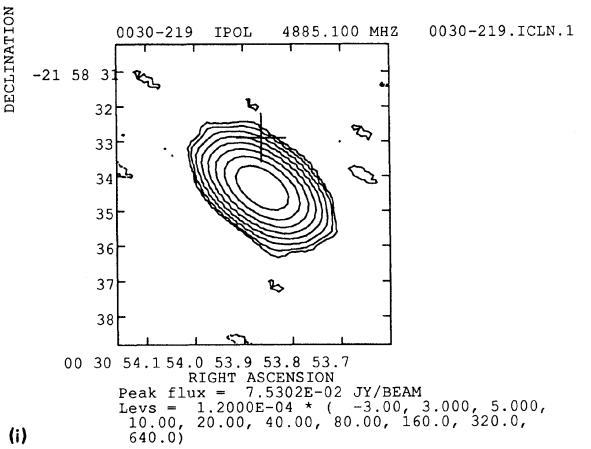

(i)

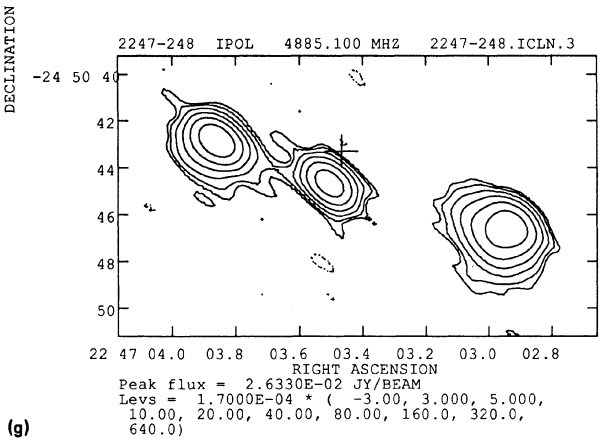

(g)

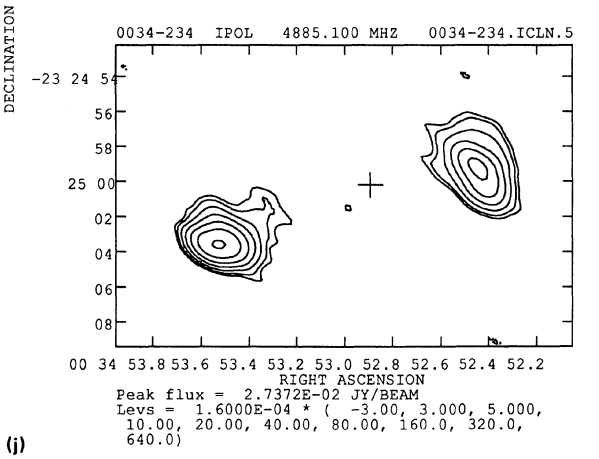

(j)

FIG. 1. (continued)

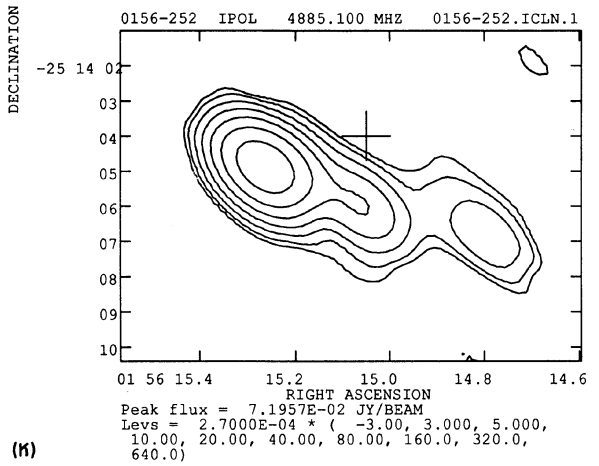

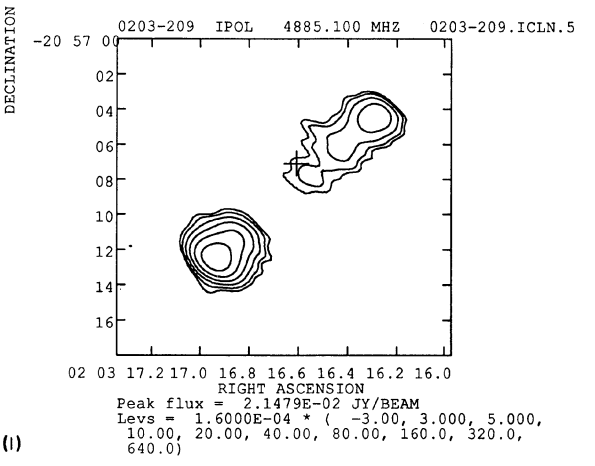

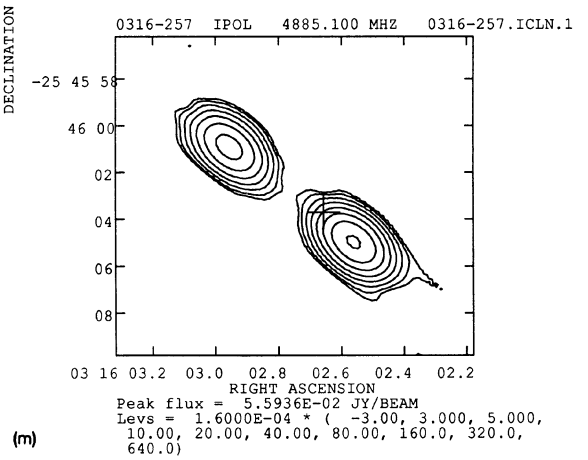

FIG. 1. (continued)

TABLE I. Radio data.

IAU Name	S(4.86) mJy	Lobe$_p$ mJy	Lobe$_f$ mJy	Core mJy	θ "	α	Log P erg/s/Hz	Log L erg/s
2025-218	86.4	53.9	33.4	-	4.0	1.09	35.7	45.83
2028-293	114.4	57.7	57.2	-	4.9	1.01	33.9	44.00
2104-242	68.6	11.3	52.3	-	21.6	1.32	35.9	46.05
2115-253	64.3	44.1	17.3	-	1.6	1.19	34.7	44.87
2200-252	94.3	44.6	49.7	-	11.4	1.05	-	-
2226-224	126.6	51.4	59.6	10.0	10.6	0.92	33.4	43.56
2247-248	100.0	45.1	32.7	21.9	13.2	0.95	35.0	45.13
2303-253	155.8	93.9	57.4	2.3	18.8	1.12	34.6	44.67
0030-219	75.4	-	-	75.4	< 1	1.07	35.3	45.44
0034-235	98.4	40.2	56.7	-	15.6	1.15	-	-
0156-252	103.1	6.9	81.0	15.5	6.6	1.05	35.5	44.26
0203-209	67.3	15.4	48 2	4.3	12.1	1.13	34.7	44.82
0316-257	93.4	57.0	35.3	-	6.7	1.13	36.1	46.19

Notes to TABLE I

1. Flux densities and powers are determined at 4.86 GHz. Powers and Luminosities are determined for $H_0 = 50$, and $q_0 = 0$.
2. θ it the largest angular size of the source in arcseconds.
3. α is the spectral index between 4680 MHz and 408 MHz.

TABLE II. Astrometric data.

IAU Name		α(1950)			δ(1950)			
2025-218	O	20	25	04.29	-21	50	54.2	
	R	20	25	04.29	-21	50	55.0	center
	H	20	25	06.69	-21	50	33.0	
2028-293	O	20	28	19.65	-29	21	44.1	
	R	20	28	19.68	-29	21	43.5	center
	H	20	28	20.90	-29	21	17.8	
2104-242	O	21	04	03.68	-24	17	16.9	
	R	21	04	03.75	-24	17	18.0	center
	A	21	04	03.48	-24	17	06.0	
2115-253	O	21	15	01.09	-25	19	11.2	
	R	21	15	01.25	-25	19	12.5	center
	B	21	15	00.02	-25	18	36.6	
2200-252	O	22	00	04.74	-25	06	27.4	
	R	22	00	04.45	-25	06	28.4	core
	A	22	00	01.63	-25	06	02.1	
2226-224	O	22	26	59.14	-22	26	08.8	
	R	22	26	59.10	-22	26	09.0	core
	A	22	27	00.00	-22	25	59.3	
2247-248	O	22	47	03.47	-24	50	43.3	
	R	22	47	03.50	-24	51	45.0	core
	A	22	47	05.51	-24	51	19.9	
2303-253	O	23	03	45.96	-25	23	05.7	
	R	23	03	45.90	-25	23	07.0	core
	A	23	03	48.59	-25	23	29.8	
0030-219	O	00	30	53.86	-21	58	32.9	
	R	00	30	53.83	-21	58	34.5	unresolved
	A	00	30	52.74	-21	59	26.3	
0034-235	O	00	34	52.89	-23	25	00.2	
	R	00	34	53.00	-23	25	01.3	center
	B	00	34	54.62	-23	24	56.1	
0156-252	O	01	56	15.05	-25	14	04.0	
	R	01	56	15.06	-25	14	06.0	core
	C	01	56	15.54	-25	13	43.4	galaxy
0203-209	O	02	03	16.61	-20	57	07.1	
	R	02	03	16.52	-20	57	07.6	core:
	D	02	03	17.33	-20	57	42.0	
0316-257	O	03	16	02.66	-25	46	03.7	
	R	03	16	02.78	-25	46	03.5	center
	A	03	16	06.95	-25	45	46.5	

c) Optical Spectroscopy

Spectroscopic observations were made with the Cerro Tololo 4 m telescope and its Folded-Schmidt spectrograph from 1–3 October 1989 (UT). We used a 150 lines/mm grating blazed at 4000 Å covering the wavelength range from 3000 to 6400 Å on 1 and 2 October. On 3 October we changed the grating tilt to cover the range 3400–6800 Å. The average pixel size was 4.3 Å×0.55″. For each galaxy observed, we offset the telescope from the secondary reference star listed in Table II. Typical integration times were 2500–3000 s. Thin cirrus clouds were present during most of the night on 1 and 2 October; 3 October was judged to be photometric. Observations of He–Ne–Ar lamps and spectrophotometric standard stars from Oke (1974) were made to calibrate the data.

The data were processed and calibrated using standard techniques and 2 d sky subtracted spectra were produced for each observation. One-dimensional spectra were extracted with a typical aperture size of 3″.5. After flux calibration the centroids, equivalent widths, and (when possible) fluxes of each of the emission lines were determined. The emission lines detected in each object are detailed below.

d) Lyman α Imaging

After the determination of redshifts additional imaging observations were made at Las Campanas in November 1989. The primary purpose of these observations was to obtain Lyman α emission-line images of the five galaxies found to have $z > 2$. Additional broadband continuum observations of some of the objects were also obtained. The emission-line images were obtained with interference filters centered near the observed wavelength of Lyα. These filters all have peak transmissions of 50%–65% and are blocked to better than 0.1%. The following emission-line observations were obtained: 2104 – 252, 7800 s, 4265/50 Å filter; 2025 – 252, 4500 s, 4450/50 Å filter; 0156 – 252, 8000 s, 3700/100 Å filter; 0030 – 252 4000 s, 3875/50 Å filter; and 0316 – 252 6000 s, 5000/100 Å filter. Each individual integration was typically 3000 s. 0030 – 252, the source with the weakest Lyα emission was not convincingly detected in a single 4000 s integration and thus was judged to be too faint to warrant additional imaging observations. All of the other objects were well detected and exhibited a variety of morphologies. Observations of twilight sky were made for use in flattening the data and spectrophotometric standard stars were observed for flux calibration. The interference filter images recorded a large number of cosmic-ray events. These were removed and were replaced by interpolating along rows. Poor charge transfer at low background levels often resulted in substantial bleeding of charge associated with these events along the CCD columns. After flattening, the individual exposures of each object were shifted into registration and added.

III. RESULTS

We describe the imaging and spectroscopic results for individual objects below. Redshifts and photometric properties of each object are listed in Table III.

2025–218. This object shows four strong emission lines [Fig. 3(b)] that we identify as Lyα, N V 1240, C IV 1549, and He II 1640. The mean redshift (excluding N V 1240) is 2.627. The N V 1240 line, which is clearly seen on both of the two-dimensional spectra, has a redshift that is 2000 km/s larger than the other lines and is quite broad (FWHM ~ 3000 km/s). The velocity width of Lyα is ~ 1700 km/s. The equivalent width of Lyα is 350 Å corresponding to a rest frame W_λ of 97 Å. The Lyman α image (Fig. 4 [Plate 89]) shows emission extended north–south over ~4″. The Lyman α emission is distributed bimodally with two peaks that correspond roughly with the two radio lobes.

2028–293. This galaxy is one of the brightest in the sample. The continuum image is extended and is roughly aligned with the axis of its double-lobed radio source. The galaxy was observed spectroscopically during evening twilight. The spectrum showed two strong emission lines that we identify as [O II] 3727 and [Ne III] 3869. The derived redshift is 0.503 and the equivalent width of [O II] 3727 is 270 Å (180 Å rest). The [O II] emission is extended along the slit, which was aligned along the long axis of the galaxy in position angle 150°.

2104–242. This object has the most extended and spectacular morphology of the sample objects observed to date. The broadband image shows two fairly distinct clumps that lie between, and are aligned with the two radio lobes. The lack of a radio core detection prevents us from determining which of the two components contains the active nucleus. The total extent of the continuum is 12″, corresponding to 135 kpc for the $H_0 = 50$, $q_0 = 0$. Two spectra were obtained

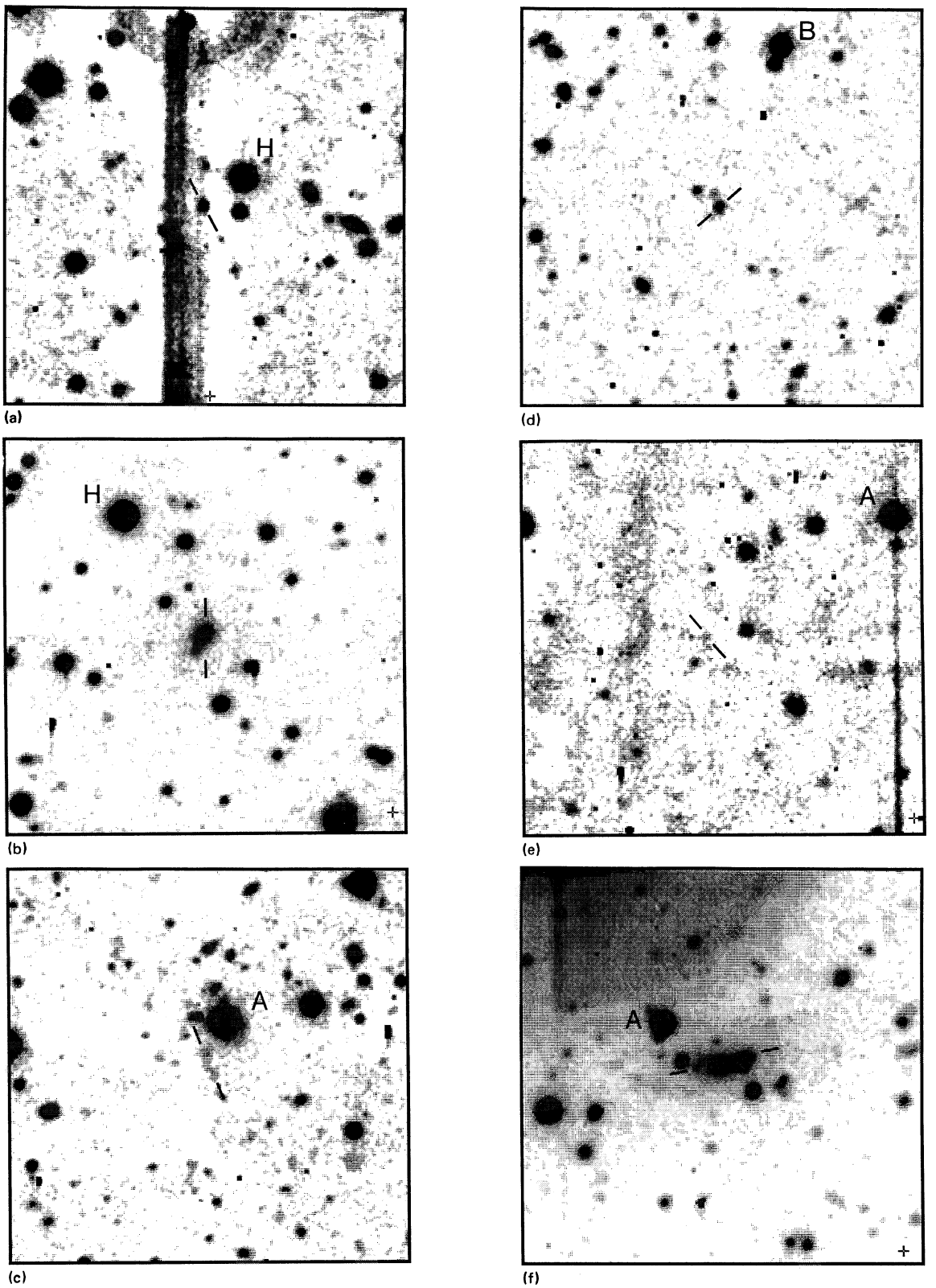

FIG. 2. (a)–(d) Gunn–Thuan *r* images of 2025 – 218, 2028 – 293, 2104 – 242, and 2115 – 253. In each field the object is marked with two dashes oriented in the same position angle as the radio source. The offset star in each field is marked with a capital letter. Each frame is 85″ on a side with north at the top and east to the left. The positions of the identifications and the offset stars are given in Table II. (e)–(h) Gunn–Thuan *r* images of 2200 – 252, 2226 – 224, 2247 – 248, and 2303 – 252. The parameters are the same as for Figs. 2(a)–2(d). (i)–(l) Gunn–Thuan *r* images of 0030 – 219, 0034 – 235, 0156 – 252, and 0203 – 209. The parameters are the same as for Figs. 2(a)–2(d). (m) A Gunn–Thuan *r* image of 0316 – 257. The image is 126″ on a side with north at the top and east to the left. The offset star, "A," is marked.

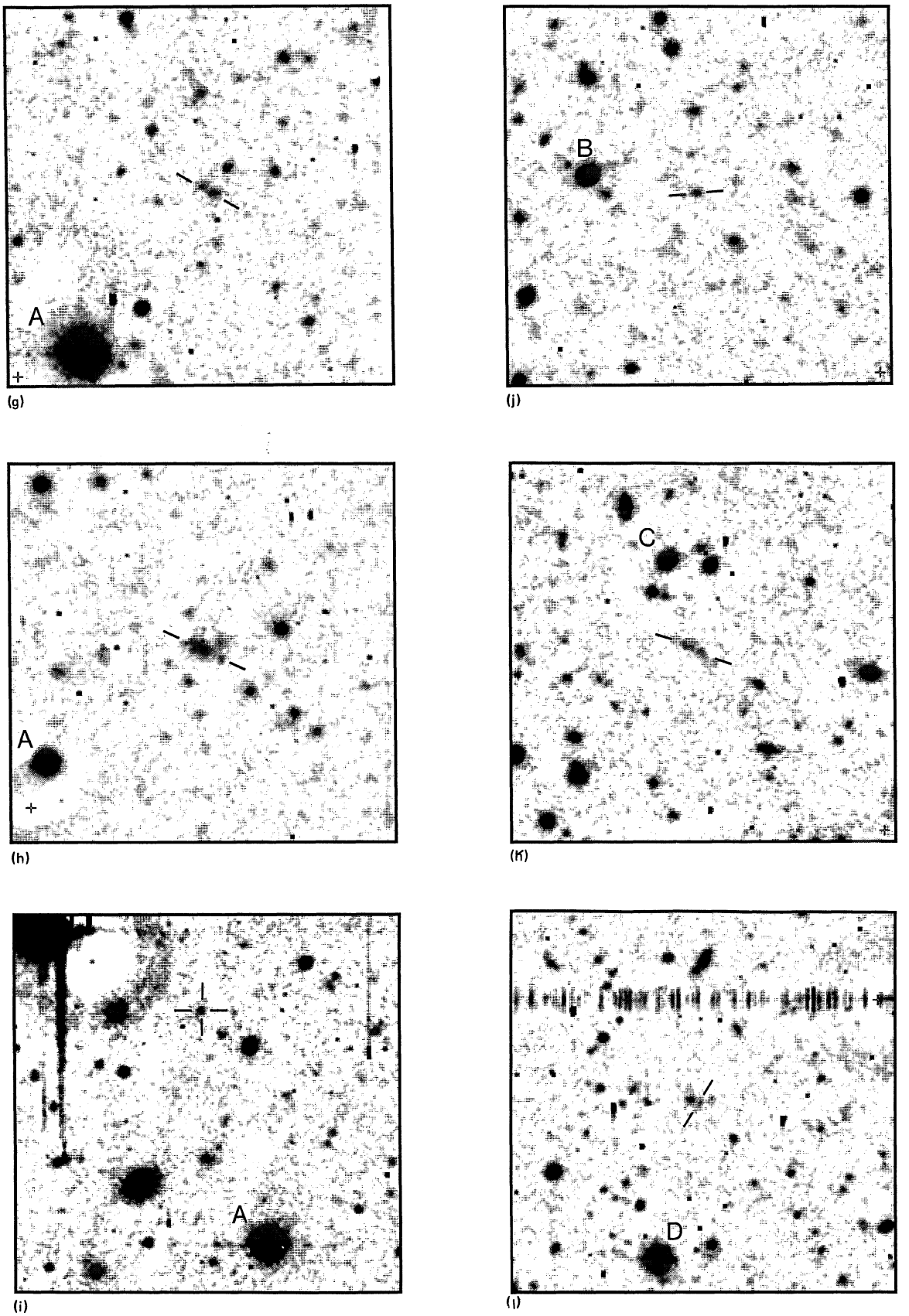

FIG. 2. (continued)

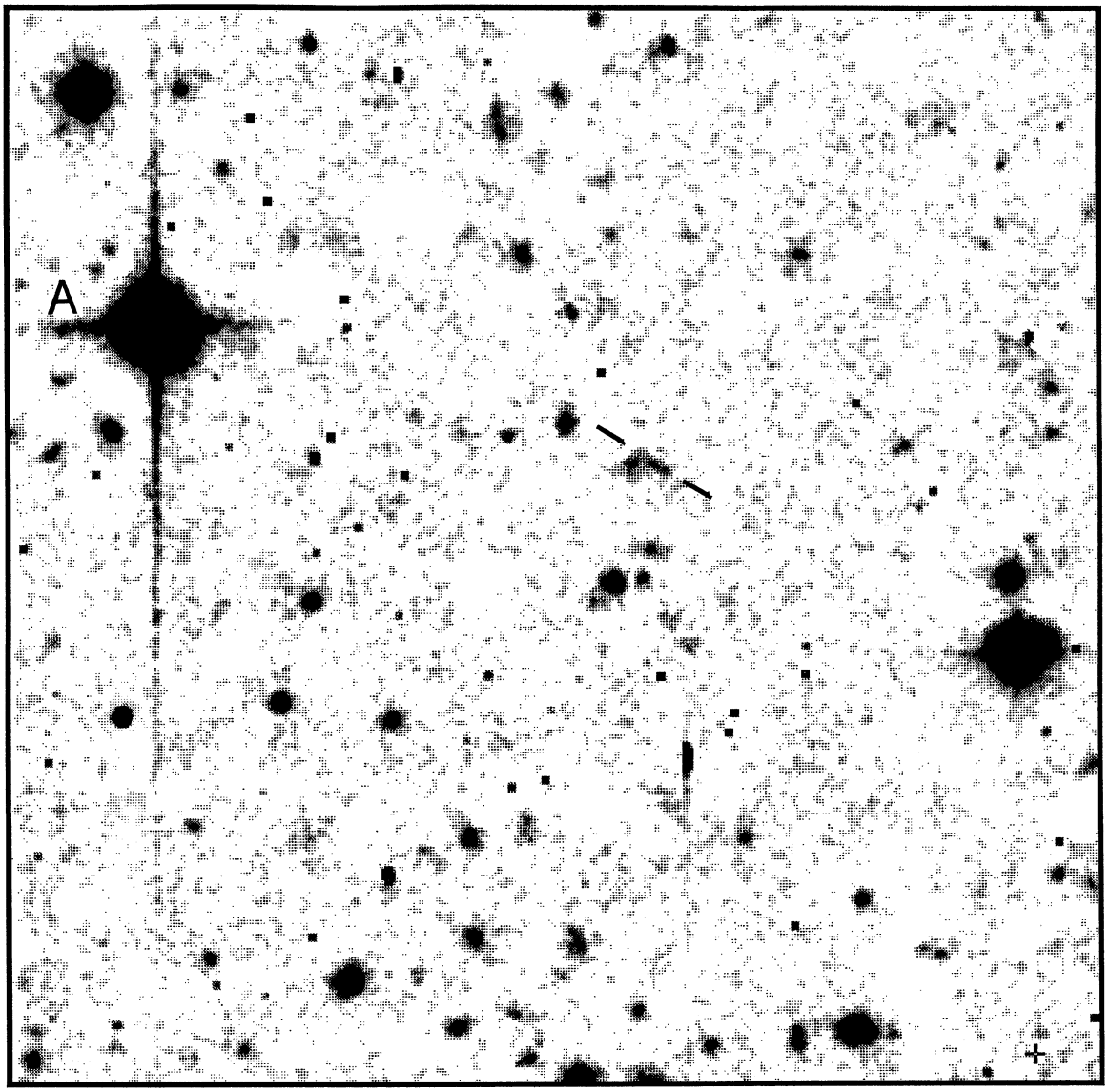

FIG. 2. (continued)

TABLE III. Spectroscopic data.

IAU Name	z	r	f(Line)	W_λ(rest)	L(Line)	Line
2025-218	2.630	22.4	2.0	97	44.50	Ly α
2028-293	0.503	20.0	2.7	180	42.65	[OII]λ3727
2104-242	2.491	23.0	5.9	445	44.89	Ly α
2115-253	1.114	22.7	3.7	47	43.68	CIII]λ1909
2200-252	—	24.9	—	-	-	
2226-224	0.28	19.5	—	-	-	
2247-248	1.634	24.1	0.7	> 400	43.42	Ly α
2303-253	0.740	21.4	0.6	30	42.42	CIII]λ1909
0030-219	2.168	24.1	0.53	174	43.66	Ly α
0034-235	—	23.6	—	-	-	
0156-252	2.016	22.7	1.5	120	44.02	Ly α
0203-209	1.258	24.7	0.67	40	42.10	CIII]λ1909
0316-257	3.13:	23.6	0.24	> 240	43.82	Ly α

Notes to TABLE III

1. Fluxes are in units of 10^{-15} erg s^{-1} cm^{-2}.
2. Equivalence widths in angstroms in the rest frame.
3. Line luminositics are computed for $H_0 = 50$, and $q_0 = 0$ in units of erg s^{-1}.

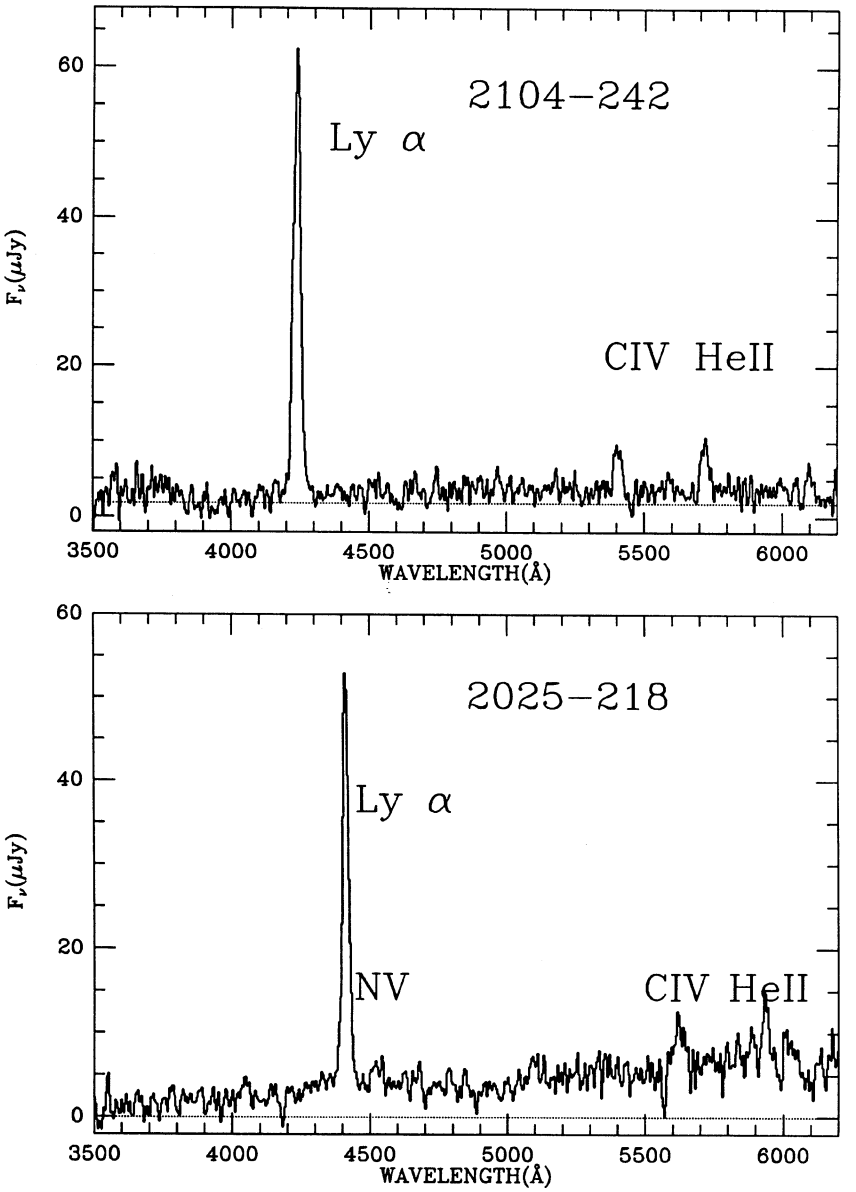

FIG. 3. One-dimensional spectra of 2104 − 242 ($z = 2.49$) and 2025 − 218 ($z = 2.63$). The Lyman α, C IV 1549, and He II 1640 emission lines are marked. The flux-density scale is in micro-Janskys.

on 1 October 1989; in both cases the slit was aligned along the two continuum clumps in position angle 21°. An additional spectrum was obtained on 3 October 1989 in the same position angle. The spectra show highly extended emission lines associated with both continuum knots. Three lines that we identify as Lyα, C IV 1549, and He II 1640 at a mean redshift of 2.490 are clearly seen in both components [Fig. 3(a)]. The northern of the two components shows a substantial velocity gradient along the slit. The mean velocity difference between the two components is 500 km/s. Both components have large Lyα equivalent widths, the northern component has $W_{\text{observed}} = 1160$ Å while the southern component has $W_{\text{observed}} = 1960$ Å. These correspond to rest-frame equivalent widths of 330 and 560 Å. The Lyman α image (Fig. 5) [Plate 90]) shows emission extended over more than 15″ (170 kpc) along the radio axis. The emission is resolved into three more or less distinct clumps, two of which correspond roughly to the two continuum objects. The third component, lying ~3″ east of the southern continuum object, has no associated continuum feature. In addition to the three distinct components there appears to be a low surface-brightness halo of emission surrounding the entire object.

2115−253. This galaxy is fairly bright and shows little extended structure in the optical continuum. Spectroscopically we detect four emission lines [Fig. 6(a)] that we identify as C III] 1909, C II] 2326, [Ne IV] 2426, and Mg II 2800 at a mean redshift of 1.114. Mg II 2800 is unusually strong in this object compared to most high-redshift radio galaxies.

2200−252. This is one of the faintest objects in that sample imaged to date. Two 3000 s spectroscopic integrations, made in mediocre conditions, failed to result in the detection of any emission lines.

2226−224. One of the brightest objects in the sample, this object has highly extended continuum that is nearly one-to-one correlated with its triple radio structure. This is one of

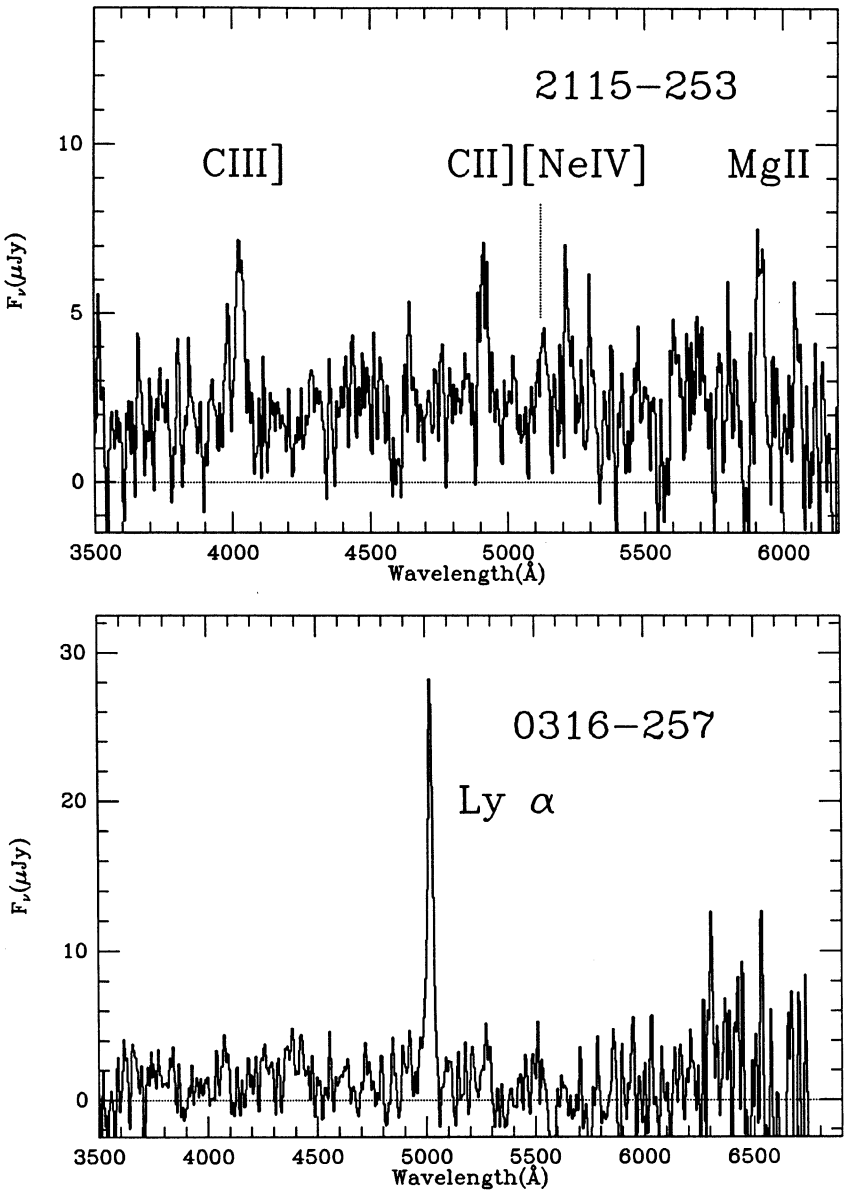

FIG. 6. One-dimensional spectra of 2115 − 253 ($z = 1.114$) and 0316 − 257 ($z = 3.13$). The prominent emission lines are marked. The flux-density scale is in micro-Janskys.

the brightest objects showing the alignment between the continuum and radio axis. An 1800 s integration, however, failed to result in the detection of any emission lines. The continua of all three components were well detected, and all are quite red. We derive a continuum redshift of 0.28 for the central component on the basis of the 4000 Å break and Ca II H and K. The western component shows evidence for the 4000 Å break, but at a low significance level. The eastern component is too faint to allow a detection of the 4000 Å break in our spectra.

2247−248. The identification is a faint galaxy showing double morphology aligned with the radio axis. One strong emission line at 3204 Å was detected as were two weaker features in a single 3000 s exposure. The 3204 Å line has an equivalent width of >1000 Å, making Lyα at $z = 1.63$ the most likely identification. The two weaker lines then agree well with identifications as C IV 1549 and C III] 1909 giving a mean redshift of 1.635. He II 1640, normally comparable to C IV 1549 is not detected, but the signal-to-noise ratio is sufficiently poor as to be consistent with C IV/He II being only 2–3.

2303−253. This galaxy is moderately faint and has a highly extended continuum morphology. The extended continuum is aligned with the triple radio source and has a strong component for component correspondence. A single 2500 s spectrum revealed three emission lines that we identify as C III] 1909, C II] 2326, and Mg II 2800 at a redshift of 0.740. The redshift was confirmed by taking a narrowband

image at the expected wavelength of [O II] 3727. Strong and highly extended emission was detected in this image, although the seeing was rather poor.

0030—219. The galaxy is rather faint and is not particularly extended. The radio source is also unresolved, although the radio spectrum is steep. The optical spectrum has three high equivalent-width emission lines that we identify as Lyα, C IV 1549, and He II 1640 at a redshift of 2.168. Lyα has an observed equivalent width of 550 Å, corresponding to $W_{\rm rest}$ = 174 Å. The emission lines are extended along the slit with a large velocity shear to the red.

0034—235. This object is nearly stellar and moderately faint. A single 3000 s spectrogram resulted in a detection of the continuum but no emission lines in the region 3100–6400 Å.

0156—252. This object is composed of three or more components that lie along the radio axis and roughly correspond to the radio core and the two radio lobes. This is one of the most extreme examples of the alignment effect in our sample. A 2500 s spectrogram revealed three emission lines that we identify as Lyα, C IV 1549, and He II 1640 at a redshift of 2.016. The lines are narrow and were extended along the slit which was oriented along the long axis of the galaxy. The Lyα image (Fig. 7 [Plate 91]) shows emission coincident with all three components of the continuum, but the highest surface-brightness Lyα lies east of the northern radio lobe. This component is several times brighter in Lyα than the radio core. The radio source also has a large asymmetry in its flux-density distribution with the northeast lobe being $\sim$10 times stronger than the southwest lobe. Strong correlations between the emission-line asymmetries and the radio-source arm length and lobe brightness asymmetries have been found by McCarthy, van Breugel, and Kapahi (1991).

0203—209. This object has a diffuse morphology that may result from contamination by foreground objects. A single spectrogram resulted in the detection of three emission lines that we identify as C IV 1549, He II 1640, and C III] 1909 at a redshift of 1.258.

0316—257. This object is faint and extended along the axis of its double radio source. A 4000 s spectrum taken on 2 October 1989 resulted in the detection of a single strong emission line at 5020 Å [Fig. 6(b)]. This line has an equivalent width greater than 1000 Å making Lyα at a redshift of 3.13 the most likely identification. The only other plausible identification is with [O II] 3727 at $z = 0.35$. A 4500 s integration was performed on 3 October 1989, in this case with the grating tilt adjusted as to cover the expected location of C IV for $z = 3.13$, and [O III] 5007, 4959 for $z = 0.34$. This spectrum confirmed the strong emission line at 5020 Å but failed to detect any additional lines. The lack of a detection of C IV 1549 does not rule out the identification of the high equivalent width line as Lyα at $z = 3.13$, but the lack of a detection of the [O III] lines or Hβ argues strongly against the high W_λ line being [O II] 3727 equivalent widths of 900 Å are unprecedented in active galaxies, and if such were the case one would certainly expect to detect the nebular lines easily. Furthermore, the alignment of the optical continuum and the radio source is phenomenon that appears to be exclusive to redshifts greater than 0.5. Thus we are quite confident in our identification of the single emission line as Lyα at $z = 3.13$. The emission-line image (Fig. 8 [Plate 92]) shows a single component that is not significantly extended. This emission is coincident with the continuum object that lies between the two radio lobes. The object to the northeast and oriented normal to the radio axis appears to lie in the foreground as its continuum is well detected below 912 Å in the $z = 3.13$ rest frame of the western object.

IV. DISCUSSION

There are a number of properties that distinguish high-redshift radio galaxies from those of the present day, although one should bear in mind that they differ in radio luminosity by 3–4 orders of magnitude. From an optical perspective distant radio galaxies differ from the present day population in their morphologies (many are multimodal and nearly all are aligned with their radio-source axes) and in their blue rest-frame colors. Luminous radio galaxies at large redshifts have rest-frame ultraviolet excesses compared to non-evolving populations of a few magnitudes or more (Lilly and Longair 1984; Eisenhardt and Leibofsky 1987). The large near-IR to rest frame UV colors are taken as the signature of an underlying old stellar population (e.g., Lilly 1988, 1989). This is difficult to reconcile with the alignment of the K band light with the radio axes (Chambers, Miley, and Joyce 1988; Eisenhardt and Chokshi 1990), but more detailed spatially resolved photometry is required to assess the significance of this properly. Younger models that reproduce to observed spectral energy distributions have recently been proposed by Chambers and Charlot (1990).

Our sample was selected by imposing a steep spectral index criterion similar to (but not quite as steep as) that used by Chambers, Miley, and van Breugel (1987). Observations of samples with flatter radio spectra and faint optical counterparts are underway. These new samples will allow us to examine the impact of the steep spectrum selection more effectively than our current sample. We note, however, that a number of the high-redshift radio galaxies in our sample have relatively strong central components (e.g., 2247 − 248). We identify these as cores on the basis of their compactness and coincidence with the optical identifications. In 0030 − 219 ($z = 2.168$) the radio source consists of a single compact component and yet has a steep spectrum ($\alpha = 1.07$). Further multifrequency observations are warranted to determine the spectra of these central components and to search for small scale extended steep spectrum emission. In contrast, strong central components are quite rare in the high- redshift 3CR galaxies (Strom *et al.* 1990; van Breugel and McCarthy 1990; Kapahi and Murphy 1990).

The optical identifications show a wide range of morphologies. A few objects (e.g., 0030 − 219, 2215 − 253, 2200 − 252) show little or no extended structure. The remaining objects, however, all show the highly elongated extended continuum that has become the hallmark of distant radio galaxies. It is worth noting that all of the objects with extended optical continua have strong emission lines. All of these objects show strong alignment of the optical continuum with the radio-source structure. This "Alignment Effect," first discovered by McCarthy *et al.* (1987) for the complete 3CR and by Chambers *et al.* (1987) for the 4C ultrasteep spectrum sample, has been the topic of numerous recent empirical and theoretical discussions (see van Breugel and McCarthy 1990; and Chambers and Miley 1990 for reviews). McCarthy and van Breugel (1989) show that for 3CR sources the alignment effect occurs for redshifts greater than $\sim$0.8. From the 3CR sample alone, we are not able to determine if this is a genuine evolutionary effect (i.e., z dependent) or if it is determined by increasing radio luminosi-

ty. The 1 Jy samples should aid in this respect. If the alignment sets in at a specific radio luminosity (log $L \sim 10^{45}$ ergs s^{-1}, $H_0 = 50$, $q_0 = 0$ for the 3CR), it should occur at larger redshifts ($z \sim 1.3$) for the 1 Jy samples. A higher degree of completeness than we have presently achieved will be required to make such a determination, but the preliminary evidence from this sample suggests that the alignment is just as strong at $z \sim 0.7$ as in the case of the 3CR. If substantiated, this would show that the alignment is a redshift rather than luminosity dependent effect.

The high-redshift objects in our sample all have strong Lyα with rest frame equivalent widths of 100–350 Å. Their emission-line spectra are similar to other high z radio galaxies (e.g., Spinrad *et al.* 1985) in that they have strong C IV 1549, He II 1640, and C III] 1909, all with comparable strengths. In three of the $z > 2$ galaxies, the emission lines are extended over scales of $\sim 5''$ or greater.

Another issue which this sample was designed to address is the correlation between emission-line luminosity and radio luminosity in powerful radio sources. Baum and Heckman (1989) and Saunders *et al.* (1989) show that the total emission-line luminosities of FRII radio galaxies are well correlated with the luminosities of their radio sources. McCarthy, Spinrad, and van Breugel (1989) show that for the complete 3CR the emission line and radio luminosities correlate over more than four orders of magnitude. While the nearby sample of Baum and Heckman (1989) shows a correlation between the luminosities that is independent of redshift, the larger samples are completely dominated by a single flux-limited catalog, the 3CR. With the 1 Jy samples we are able to directly determine if the observed L(emission)–L(radio) correlation is primary or is a secondary result of the z–L(radio) correlation of the 3CR and an evolutionary z–L(emission) correlation. Because of the large scatter in the L(emission)–L(radio) for the complete 3CR (McCarthy *et al.* 1989) we require a large 1 Jy class sample to test for a primary L(emission)–L(radio) correlation. The data presented here, and that given by Allington-Smith *et al.* (1988), are in better agreement with a primary L(emission)–L(radio) correlation than a z–L(emission) correlation. Corroborating evidence from this comes from the reduced equivalent widths of the emission lines in the B2 1 Jy sample (Allington-Smith *et al.* 1988) and in this sample. The median W_λ (Lyα) for our sample is 200 Å (rest) while for the complete 3CR sample the median is 350 Å (rest), even though our median z is higher.

V. SUMMARY

We have presented radio and optical observations of a small sample of radio galaxies drawn from the Molonglo Reference Catalogue. Out of 13 galaxies observed we determined redshifts for 11, the median z being 1.6. We expect that our total sample of 150 sources will yield a large sample of radio galaxies with redshifts greater than 2. This sample will be used to explore the properties of radio galaxies at extreme luminosities and early epochs. Preliminary indications from the data presented here suggest that the alignment of the optical and radio continuum axes is primarily a redshift dependent effect and that the correlation between radio and emission-line luminosities is genuine rather than a secondary correlation resulting from redshift correlations in both luminosities.

We would like to thank the staffs of the Las Campanas, National Optical, and National Radio Astronomy Observatories for their expert assistance with the observations. V. K. K. acknowledges the support of a National Research Council–JPL Senior Research Associateship under which part of this research was carried out. The National Radio Astronomy Observatory and the VLA are operated by Associated Universities, Inc., under a contract with the National Science Foundation. The National Optical Astronomy Observatory and the Cerro Tololo Inter-American Observatory are operated by AURA, Inc., under a contract with the National Science Foundation. The Las Campanas Observatory is owned and operated by the Carnegie Institution of Washington.

REFERENCES

Allington-Smith, J. R. (1982). Mon. Not. R. Astron. Soc. **199**, 611.
Allington-Smith, J. R., Spinrad, H., Djorgovski, S., and Liebert, J. F. (1988). Mon. Not. R. Astron. Soc. **234**, 1091.
Baum, S. A., and Heckman, T. M. (1989). Astrophys. J. **336**, 681.
Bennet, C. R. (1962). Mem. R. Astron. Soc. **68**, 163.
Chambers, K. C., and Charlot, S. (1990). Astrophys. J. Lett. **348**, Ll.
Chambers, K. C., and McCarthy P. J. (1990). Astrophys. J. Lett. **354**, L9.
Chambers, K. C., and Miley, G. K. (1990). In *The Hubble Centennial Symposium: The Evolution of Galaxies,* edited by R. G. Kron (Astron. Soc. Pac. Conf. Ser. **10**, 373.
Chambers, K. C., Miley, G. K., and Joyce, R. (1988). Astrophys. J. Lett. **329**, L75.
Chambers, K. C., Miley, G. K., and van Breugel, W. J. M. (1987). Nature **329**, 604.
Chambers, K. C., Miley, G. K., and van Breugel, W. J. M. (1990). Astrophys. J. (in press).
Condon, J. (1984). Astrophys. J. **287**, 461.
Douglas, J., Bash, F. N., Torrence, G. W., and Wolfe, C. (1980). Univ. Tex. Publ. Astron. No. 17.
Dunlop, J. S., Peakcock, J. A., Savage, A., Lilly, S. J., Heasley, J. N., and Simon, A. J. B. (1989). Mon. Not. R. Astron. Soc. **238**, 1171.
Eisenhardt, P., and Chokshi, A. (1990). Astrophys. J. Lett. **351**, L9.
Eisenhardt, P., and Lebofsky, M. J. (1987). Astrophys. J. **316**, 70.
Gopal-Krishna, G. K. (1988). Astron. Astrophys. **113**, 150.
Kapahi, V. K., and Kulkarni V. K. (1990). Astron J. **99**, 1397.
Kapahi, V. K., and Murphy, D. W. (1990). In *Parsec-Scale Radio Jets,* edited by J. A. Zenzus and T. J. Pearson (Cambridge University, Cambridge) (in press).
Laing, R. A., and Peacock J. A. (1980). Mon. Not. R. Astron. Soc. **190**, 903.
Large, M. I., Mills, B. Y., Little, A. G., Crawford, D. E., and Sutton, J. M. (1981). Mon. Not. R. Astron. Soc. **194**, 693.
Lawrence, C. R., Bennett, C. L., Hewitt, J. N., Langston, G. I., Klotz, S. E., and Burke, B. F. (1986). Astrophys. J. Suppl. Ser. **61**, 105.
Lilly, S. J. (1988). Astrophys. J. **333**, 161.
Lilly, S. J. (1989). Astrophys. J. **340**, 77.
Lilly, S. J., and Longair, M. S. (1984). Mon. Not. R. Astron. Soc. **211**, 833.
McCarthy, P. J., Spinrad, H., and van Breugel (1989). In *Active Galactic Nuclei,* edited by D. E. Osterbrock, and J. Miller (Kluwer, Academic), p. 543.
McCarthy, P. J., and van Breugel, W. J. M. (1989). In *The Epoch of Galaxy Formation,* edited by C. Frenk, R. S. Ellis, T. Shanks, A. F. Heavens, and J. A. Peacock (Kluwer, Dordrecht), p. 57.
McCarthy, P. J., van Breugel, W. J. M., and Kapahi, V. K. (1991). As-

trophys. J. (in press).
McCarthy, P. J., van Breugel, W. J. M., Spinrad, H., and Djorgovski, S. G. (1987). Astrophys J. Lett. **321**, L29.
Oke, J. B. (1974). Astrophys. J. Suppl. Ser. **27**, 21.
Peacock, J. A. (1985). Mon. Not. R. Astron. Soc. **217**, 601.
Robertson, J. G. (1973). Aust. J. Phys. **26**, 403.
Saunders, R., Baldwin, J. E., Rawlings, S., Warner, B., and Miller, L. (1989). Mon. Not. R. Astron. Soc. **238**, 777.
Spinrad, H., Filippenko, A. V., Wyckoff, S., Stocke, J. T., Wagner, R. M., and Lawrie, D. G. (1985). Astrophys. J. Lett. **299**, L7.
Strom, R. G., Riley, J. M., Spinrad, H., van Breugel, W. J. M., Djorgovski, S., Liebert, J. F., and McCarthy, P. J. (1990). Astron. Astrophys. **227**, 19.
Tielens, A. G. G. M., Miley, G. K., and Willis, A. G. (1979). Astron. Astrophys. Suppl. **35**, 153.
van Breugel, W. J. M., and McCarthy, P. J. (1990). In *The Hubble Centennial Symposium: The Evolution of Galaxies,* edited by R. G. Kron, Astron. Soc. Pac. Conf. Ser. **10**, 359.
Windhorst, R. A. (1990). In *The Hubble Symposium on Galaxies,* edited by R. G. Kron, Astron. Soc. Pac. Conf. Ser. **10**, 389.
Windhorst, R. A., Kron, R. G., and Koo, D. C. (1984). Astron. Astrophys. Supl. Series **58**, 39.

PLATE 89

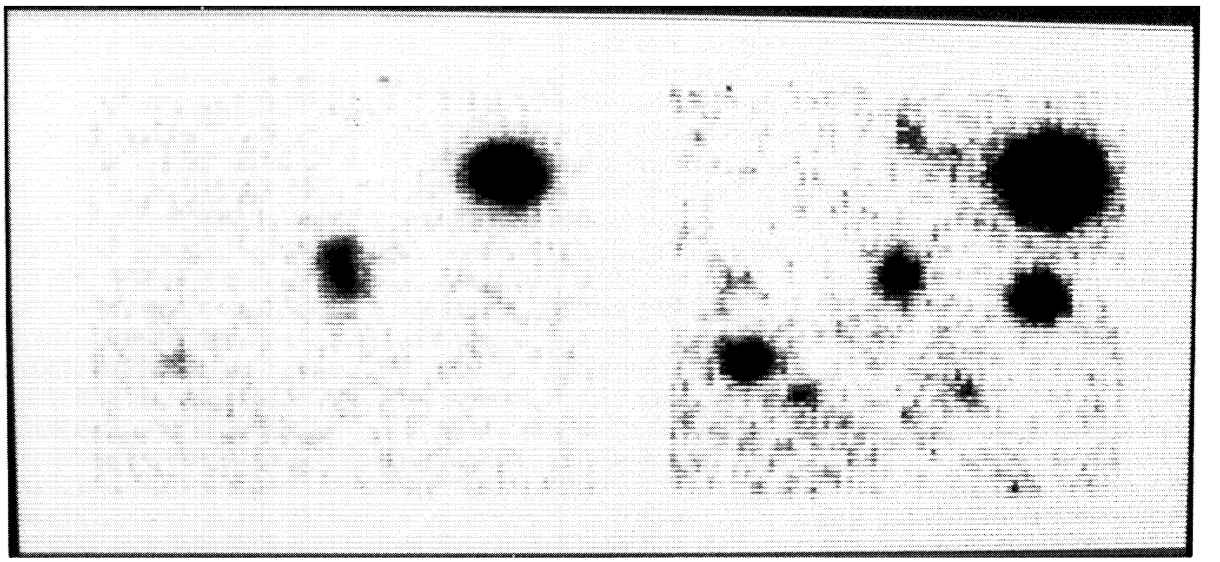

FIG. 4. Lyman α and r images of 2025 − 218 ($z = 2.630$). The images are both 25″ on a side and are in mutual registration. The star to the upper right is the offset star H. The total extent of Lyα is 4″ and corresponds roughly to the size and position angle of the radio source.

McCarthy *et al.* (see page 1019)

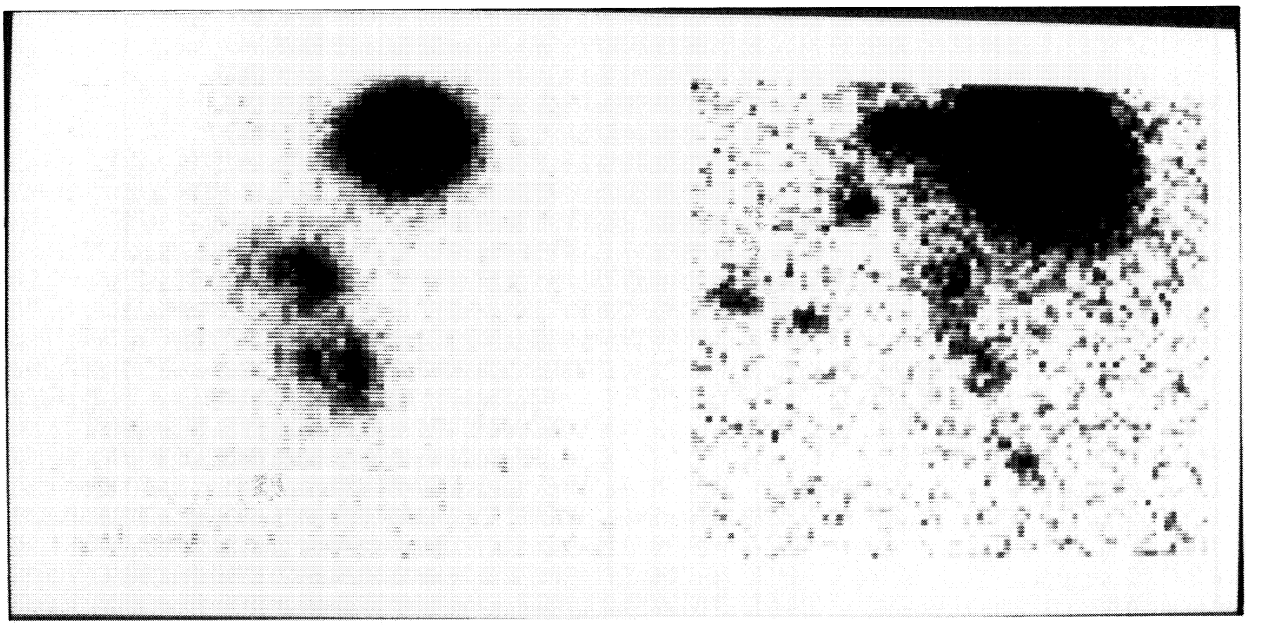

FIG. 5. Lyman α and r images of 2104 − 242 ($z = 2.491$). The images are both 25″ on a side and are in mutual registration. The star to the upper right is the offset star A. The total extent of the Lyα emission is 15″ × 5″ (170 × 60 kpc).

McCarthy *et al.* (see page 1023)

PLATE 91

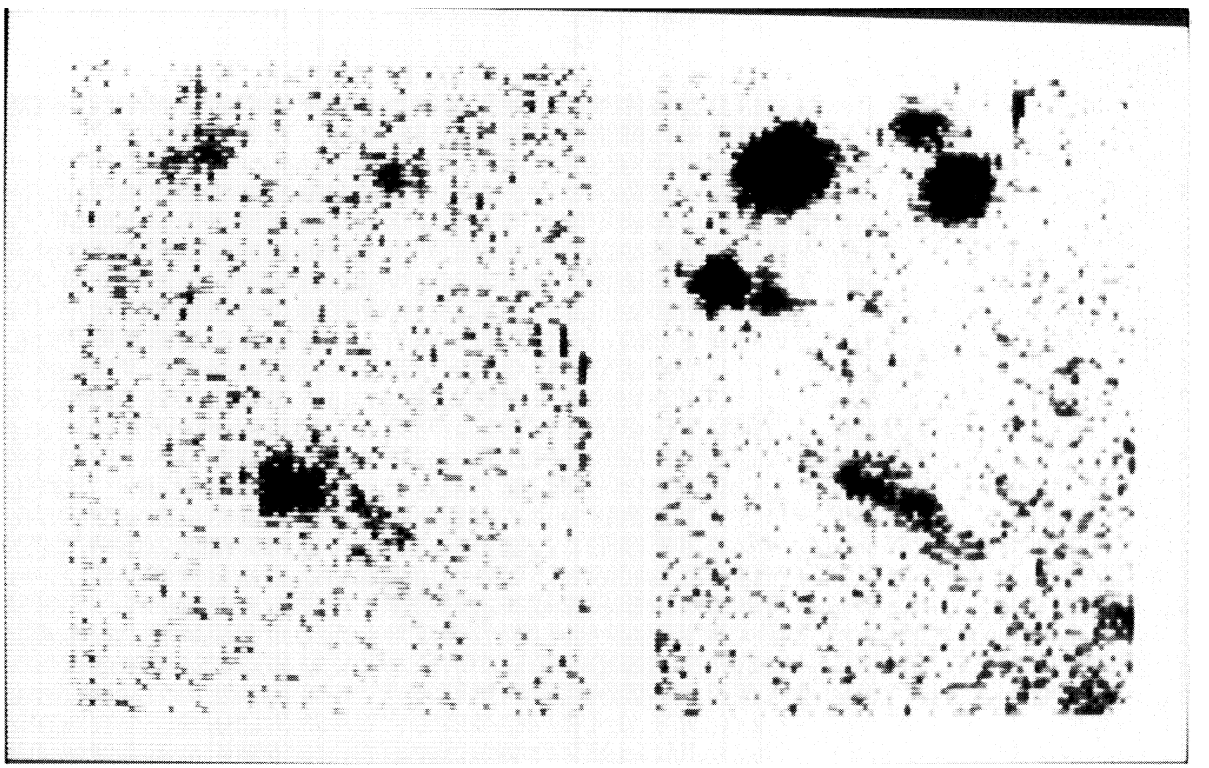

FIG. 7. Lyman α and r images of 0156 − 252 ($z = 2.016$). The images are both 27″ × 40″ and are in mutual registration. The galaxy to the upper left is the offset object C. The total extent of the Lyα emission is 9″ × 4″ (100 × 45 kpc) and the extent of the continuum in ~11″ × 3″ (130 × 35 kpc).

McCarthy *et al.* (see page 1025)

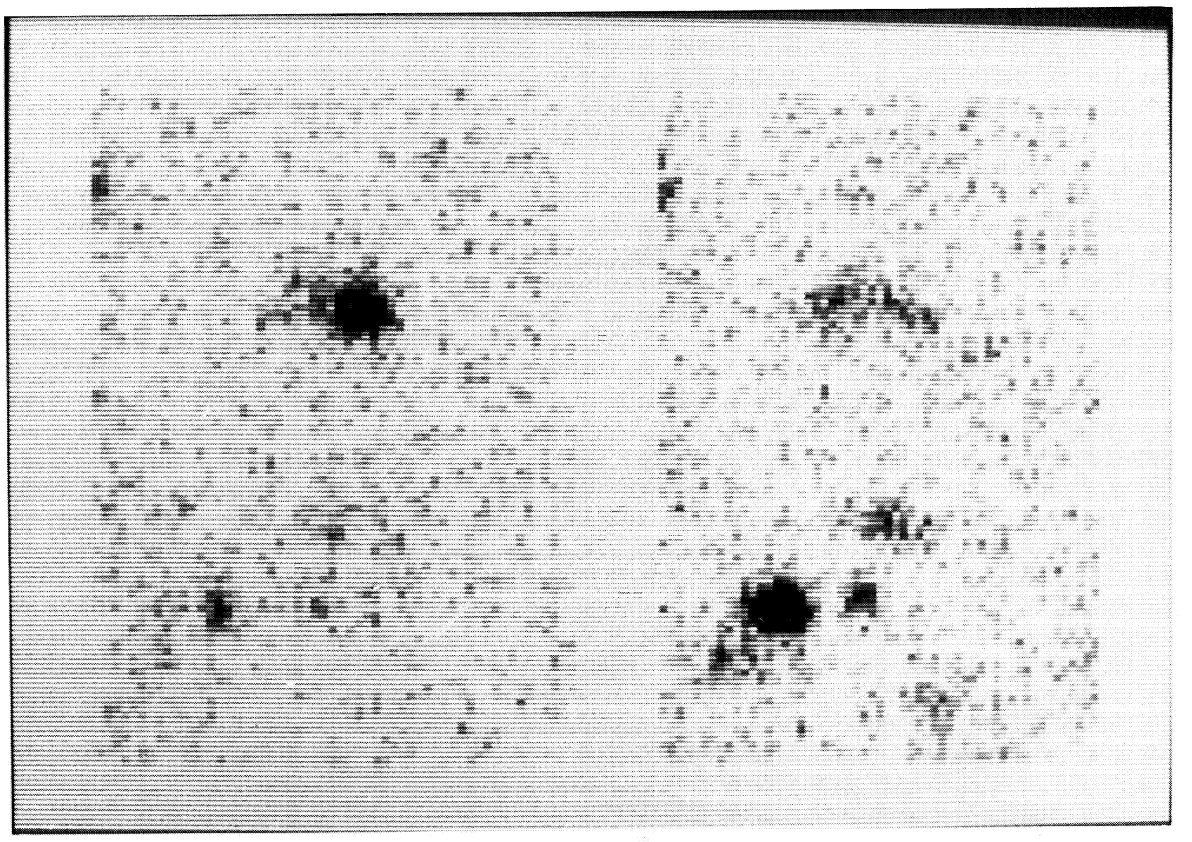

FIG. 8. Lyman α and r images of 0316 − 257 ($z = 3.13$). The images are 20″ × 33″ and are in mutual registration. The Lyα emission is smaller than ~2″ and lies between the two radio lobes. The object 4″ to the east is believed to lie in the foreground.

McCarthy *et al.* (see page 1025)